Synthesis, Characterization, and Double Layer Capacitance Charging of Nanoclusters Protected by 6-Mercaptopurine

ARTICLE *in* THE JOURNAL OF PHYSICAL CHEMISTRY C · MARCH 2009

Impact Factor: 4.77 · DOI: 10.1021/jp810720t

4 AUTHORS, INCLUDING:

Rafael Madueño
University of Cordoba (Spain)
24 PUBLICATIONS **540** CITATIONS
SEE PROFILE

Manuel Blázquez
University of Cordoba (Spain)
76 PUBLICATIONS **882** CITATIONS
SEE PROFILE

Teresa Pineda
University of Cordoba (Spain)
41 PUBLICATIONS **325** CITATIONS
SEE PROFILE

THE JOURNAL OF PHYSICAL CHEMISTRY C

Article

Synthesis, Characterization, and Double Layer Capacitance Charging of Nanoclusters Protected by 6-Mercaptopurine

Alfonso J. Viudez, Rafael Maduen#o, Manuel Bla#zquez, and Teresa Pineda

J. Phys. Chem. C, **2009**, 113 (13), 5186-5192• DOI: 10.1021/jp810720t • Publication Date (Web): 11 March 2009

Synthesis, Characterization, and Double Layer Capacitance Charging of Nanoclusters Protected by 6-Mercaptopurine

Alfonso J. Viudez, Rafael Madueño, Manuel Blázquez, and Teresa Pineda*

Departamento de Química Física y Termodinámica Aplicada, Universidad de Córdoba, Campus de Rabanales, Ed. Marie Curie, E-14071 Córdoba, Spain

Received: December 5, 2008; Revised Manuscript Received: January 16, 2009

The synthesis of gold nanoparticles by using the one-phase method of Brust has been carried out in this work to obtain 6-mercaptopurine monolayer protected gold nanoclusters (6MP-MPCs). The 6MP-MPCs are somewhat polar clusters that are soluble in polar solvents such as DMF and DMSO and in neutral and alkaline aqueous solutions. The average size of the clusters is 2.4 ± 0.5 nm and a stoichiometry of $Au_{459}(6MP)_{62}$ has been established by taking into account high resolution transmission electron microscopy, X-ray diffraction, and thermogravimetric analysis results of the 6MP-MPCs. The mode of binding of the 6MP molecules to the gold surface has been studied by FT-infrared and X-photoelectronic spectroscopies that evidence the existence of the S−Au interaction. Moreover, the different tautomers of the 6MP molecules in homogeneous solution suffer the transformation into the thiol N(9)H tautomer in the adsorbed state. Finally, taking together the size of these MPCs with the low effective dielectric constant of the 6MP monolayer in contact with the DMF solution makes the observation of the quantized charging of the double layer of these 6MP-MPCs possible. A capacitance value of 1.06 aF consistent with the core dimension and protective monolayer dielectric properties has been determined for the individual 6MP-MPCs.

Introduction

The investigation of the electronic properties and chemical reactivities of monolayer-protected metallic nanoclusters (MPCs) can be conveniently carried out by controlling their size as well as their size dispersion.[1−4] One of the major factors that contribute to this point is the chemical nature of the capping agent that provides a means to tune the cluster size and, moreover, the chemical properties of these MPCs. Most of the work in this field has been made with gold and alkane or nonpolar aromatic thiol derivatives. Thus, some variations of the synthetic two phase method first described by Brust et al.[5] have been employed in order to easily get MPCs that are stable against aggregation when dried of solvent and that can be repeatedly isolated and redissolved.[6−9] These synthetic methods produce MPCs with a preferred core size, but in most cases, they exhibit polydispersity. Therefore, a large fraction of research has been focused on studies dealing with MPC core uniformity and the different separation methods employed.[10−15]

The potential bioanalytical and biomedical applications of MPCs has made many groups interested in the synthesis of water-soluble MPCs[10−13,16,17] and some of them have been reported including tiopronin-[16,17] and glutathione-protected Au MPCs.[10,11,13] The preparation of these water-soluble MPCs is carried out by the single phase method that avoids the extraction of the water-soluble ligand to the aqueous phase.[18] Then, the choice of the reaction solvent for this synthesis is a major issue since not only the solubility of the ligands but also the solubility and stability of the MPCs produced are important.

Our group has been exploring the formation and characterization of 6-mercaptopurine (6MP; Chart 1) self-assembled monolayers (SAMs) on Au(111) single crystal electrode.[19−22] This research has recently been extended to studies of these SAMs adsorbed on 13 nm gold nanoparticles (AuNPs).[23] In this study, the AuNPs were synthesized by the classic reduction method by using citrate as a capping and protecting agent,[24] and in a second step, the citrate anions adsorbed on the nanoparticle surface were displaced by the 6MP molecules. These nanoparticles, the 6MP−AuNPs, were stable in neutral and alkaline solutions, whereas they suffered reversible agglomeration in acid medium. The binding of 6MP to the gold nanoparticle surface takes place by sulfur interaction and probably by a weaker interaction through the N7 atom of the indole ring. These features have been observed by FT-IR spectroscopy and are in agreement with the mode of binding of 6MP on Au(111) surface as deduced by electrochemical means.[20] Moreover, the acid−base properties of the 6MP-SAM are maintained when passing from the 2D to 3D surface. In fact, the adsorbed 6MP molecules that should adopt the thiol tautomer conformation have a dissociation pK_a for the N(9)−H group in the pH interval of 7−8 and, this value is independent of the surface geometry (2D or 3D surfaces).[22,23]

Recently, Jadzinsky et al.[25] have reported the successful crystallization and complete X-ray structure determination of a *p*-mercaptobenzoic acid (MBA) protected gold nanoparticle ($Au_{102}(MBA)_{44}$) and have observed that the thiolate groups form linear RS−Au−RS motifs (called "staple" motifs) on the nanoparticle surface. A structural description given by Whetten and Price[26] is that the embedded Au_{102} structure is composed of a grand core of 79 Au atoms plus 23 exterior Au atoms that serve only to connect the thiolate groups with the 79 atom grand

CHART 1: 6-Mercaptopurine Structure and Numbering

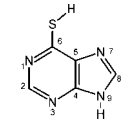

* Corresponding author. Phone: +34-957-218646. Fax: +34-957-218618. E-mail: tpineda@uco.es.

10.1021/jp810720t CCC: $40.75
Published on Web 03/11/2009

core. This finding contrasts with the accepted, standard model of the formation of single covalent bonds in which independent thiyl groups are attached directly to close-packed underlying gold substrate. The binding motif exemplifies the "divide-and-protect" model,[27] in which oligomeric aurous Au(I)−thiolate complexes interact weakly with the surface atoms of the grand core. In this picture, the thiol monolayer is stabilized not only by gold−sulfur bonding but also by interactions beween MBA molecules. These interactions can be of phenyl ring stacking in parallel or right angle configurations or between sulfur atoms with phenyl rings.[25]

Likewise, the crystal structure of the $Au_{25}(CH_2CH_2Ph)_{18}$ nanoparticle[28] shows that the organothiolate ligands are bonded in short stellated semirings, or "staples", of $Au_x(SR)_y$ chains that make them appropriate to describe the nanoparticle as a "staple-protected" Au_{13} core. The thiolate ligand attachment sites are symmetrically distributed on the surface to ensure complete passivation of the nanoparticle. It has been concluded that this gold thiolate substructure seems to be a common motif of gold cluster chemistry.[26]

In this work, we have synthesized gold nanoclusters protected by 6MP of a smaller size by following the one-phase method first described by Brust et al.[18] By using DMF as a solvent, we have found that the 6MP molecules rapidly interact with the gold nucleus surfaces and self-assemble giving place to a stable and low polidisperse preparation of gold nanoclusters. The characterization of the 6MP protected gold nanoclusters (6MP-MPCs) has been carried out by means of techniques such as transmission electronic microscopy (TEM), UV−visible, FT-IR, and XPS spectroscopies, thermogravimetric analysis (TGA), and X-ray diffraction. Finally, the quantum double layer (QDL) voltammetry of the 6MP-MPCs has been explored, pointing out the possibility of the observation of this phenomenon with MPCs capped with polar molecules.

Experimental Section

Chemicals. All these chemicals were commercially available and were used as received: 6MP, sodium borohydride, dimethylformamide (DMF), and tetrabutyl ammonium hexafluorophosphate (Bu_4NPF_6) were from Aldrich-Sigma. Hidrogen tetrachloroaurate trihydrate (from 99.999% pure gold) was prepared using a literature procedure.[29] Deionized water (18 MΩ) from milli-Q system was used in all of the experiments.

Synthesis of 6MP-MPCs. The synthesis of 6MP-MPCs was made by following a variation of the single phase system first derived by Brust el al.[18] The extremely low solubility of 6MP in apolar solvents impedes the use of the two phase synthesis. The choice of DMF as the synthesis solvent is made on the basis of the 6MP solubility and the stability of the 6MP-MPCs formed in this solvent.

The synthesis of the 6MP-MPCs was carried out by mixing 6MP (1.2 mmol in 10 mL of DMF) with $HAuCl_4$ (0.3 mmol in 6 mL of H_2O) under strong stirring conditions at a temperature of 4 °C. The solution turns red and later becomes colorless. After 30 min, sodium borohydride (3 mmol) was fastly added. The reaction mixture changes rapidly to black and then is left under stirring conditions for 1 h. All of the process is carried out at the constant temperature of 4 °C.

In order to eliminate the excess of 6MP molecules as well as other impurities, the solution containing all of the reaction components was dialyzed against a 10 mM NaOH solution. The dialysis was repeated up to the complete elimination of free 6MP molecules of the sample. The cleaning procedure was followed by UV−visible spectroscopy of the dialysis solution and finally by measuring the UV−visible spectrum of the 6MP-MPC sample. As can be seen in Figure 1, the spectrum shows a plasmon band centered at 526 nm and a small shoulder at around 310−315 nm due to the 6MP absorption under these conditions. An alternative method to eliminate impurities was centrifugation, but the high stability of the 6MP-MPCs in DMF or in alkaline aqueous solutions precludes the precipitation in a short time and turned out to be a tedious process. The use of different solvents was also proved, but a parallel behavior of solubility of 6MP-MPCs and 6MP molecules renders the impurities difficult to be eliminated from the sample.

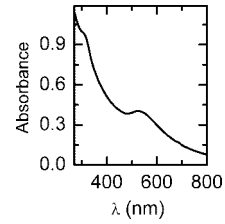

Figure 1. UV−visible spectrum of 6MP-MPCs in NaOH 0.01 M.

Methods. UV−visible spectra were collected with a Jasco UV−visible−NIR (model V-570) spectrometer. Infrared measurements of solid samples (KBr) were conducted with a Brucker (model Alpha T) spectrometer.

X-photoelectronic spectroscopy (XPS) analyses were performed with a SPECS Phoibos 150 MCD spectrometer using nonmonochromatized (12 KV, 300 W) Mg Kα radiation (1253.6 eV). An amount of dry solid 6MP-MPCs was pressed in a pellet and mounted on a steel sample holder and introduced directly into the XPS analytical chamber. The working pressure was $<5 \times 10^{-9}$ Pa. The spectrometer was calibrated assuming the binding energy (BE) of the Au $4f_{7/2}$ line at 84.0 eV. The standard deviation for the BE values was 0.2 eV. Survey scans were run in the 0−1100 eV range (pass energy 60 eV), whereas detailed scans were recorded for the Au 4f, N 1s, and S 2p regions. The analysis involved linear background subtraction, and whenever necessary, spectral deconvolution was carried out by nonlinear least-squares curve fitting, adopting a Gaussian sum function. The atomic composition of the MPC sample was calculated by peak integration, using the sensitivity factors supplied by the spectrometer manufacturer.

HR-TEM images were obtained with a JEOL JEM 2010 instrument operating at 80−200 kV and analyzed using Image Pro Plus software. Samples were prepared by casting and evaporating a droplet of MPC solution (2−3 mg/mL) onto Formvar-coated Cu grids (400 mesh, Electron Microscopy Sciences).

Thermogravimetric analysis (TGA) was performed with a Setaram Sestsys 12 system on accurately weighted, carefully dried, 15−20 mg samples. In the temperature ramp (30−800 at 30 °C/min), the organic volatilization and ensuing mass loss occurred for all samples, leaving a metal gold residue in the pan.

Powder X-ray diffraction data were obtained using a Siemens (model D5000) diffractometer with a Cu kα source operating at 40 kV and 30 mA.

Differential pulse voltammetry was performed on 0.1−0.2 mM solutions (degassed and blanketed with N_2) of 6MP-MPCs in 0.1 M Bu_4NPF_6/DMF using a CHI 900B instrument. The single-compartment electrochemical cell contained 1.6 mm diameter Pt working, Pt wire counter and Ag wire quasi-reference electrodes. The working electrode was precleaned by polishing with 0.05 μm alumina powder followed by potential-

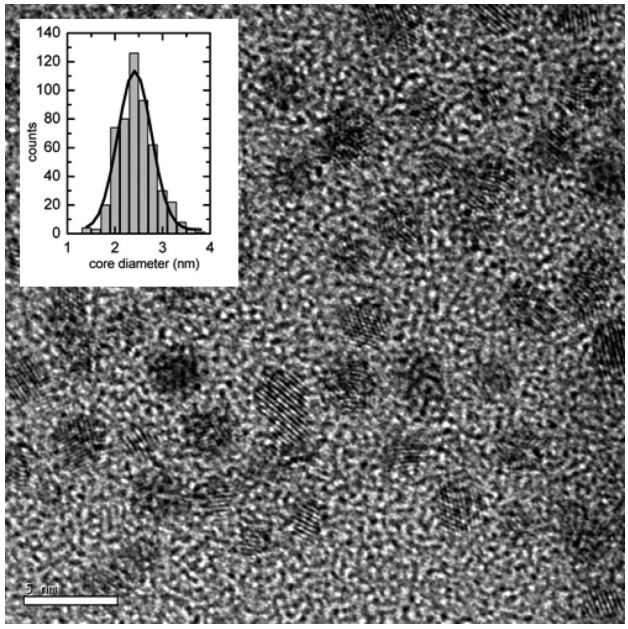

Figure 2. HRTEM micrograph of the 6MP-MPCs. Inset shows histogram of the corresponding distribution of core sizes. Scale bar is 5 nm.

cycling in 0.1 M H_2SO_4 up to the appropriate i-E profile was obtained. The Pt and Ag wire were flame annealed before use.

Results and Discussion

Preparation and Characterization of 6MP-MPCs. The low solubility of 6MP in apolar solvents makes the use of the two-phase synthesis method of Brust et al.[5] inapplicable. However, this compound is soluble in some polar solvents such as DMSO and DMF. The MPCs formed in DMSO suffered irreversible agglomeration during the synthesis procedure and became useless for any further application. We also assayed the preparation of 6MP-MPCs in DMF, and we found that this procedure is the most appropriate based on the stability of the resulting MPCs in this solvent or in aqueous solutions. Moreover, the solubility of 6MP in DMF is high enough to allow the use of a wide range of Au:6MP ratios to obtain amounts of MPCs to work with. In the present work, we were interested in the synthesis of small core MPCs and we have used a ratio of 6MP:Au of 4:1, since higher ratios did not decrease the core size of the gold clusters. Additionally, decreasing the temperature of synthesis to 4 °C helped to decrease the cluster size.

Once the 6MP-MPCs are clean, they can be dried of solvent and a black and crystalline powder is obtained that can be redissolved maintaining its initial properties.

Figure 2 shows the typical TEM images of 6MP-MPCs. The sizes of about 600 particles were measured from the TEM images, and the core sizes are plotted as a histogram. The average core diameter of the particles is 2.4 ± 0.5 nm. The marginal resolution of the Au core edges contributes to uncertainty in the apparent average core diameter. Therefore, the nanoclusters obtained by this method are close to monodispersity.

The X-ray difractogram of the solid 6MP-MPCs is shown in Figure 3. The diffraction pattern observed shows a broad peak at 38.9°. In a first approximation, it can be said that only the peak corresponding to the (111) plane reflection of gold (as referred in the JCPDS, file no. 4-0784)[30] is observed. This fact is in agreement with the XRD spectrum for the octahedral gold with a preferential orientation of the particles along (111) planes

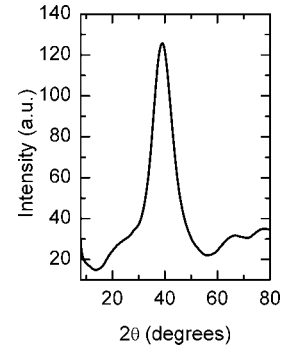

Figure 3. Powder XRD pattern of the 6MP-MPCs.

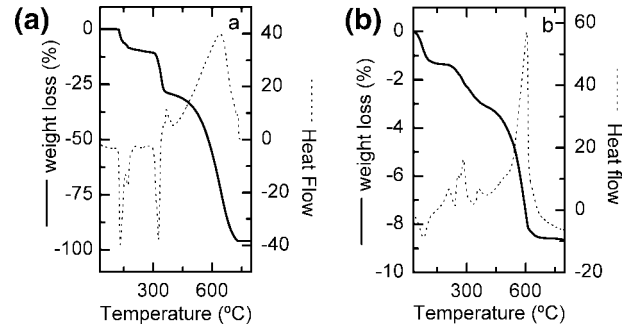

Figure 4. TGA analysis of free 6MP (a) and 6MP-MPCs (b).

parallel to the substrate.[31] However, in a deeper examination of the spectrum, a shoulder at higher reflection angles i.e., 44.5°, coinciding with the (200) reflection line for gold fcc and two small peaks at around 65° and 77.7° corresponding to the (220) and (311) reflections, can be observed. Thus, the truncated octahedra is the most likely shape of the 6MP-MPCs as judged by the diffraction pattern.[31] Taken together the results of HR-TEM and X-ray diffraction, these nanoclusters should be composed of 472[32] or 459 gold atoms.[33]

The Scherrer formula given by eq 1 was used to calculate the nanoclusters size, D

$$D = \frac{K\lambda}{B\cos\theta} \tag{1}$$

where K is the Scherrer constant, λ is the wavelength of the X-rays, B is the full width at half-maximum of the reflection peak, and θ is the diffraction angle. The B value was determined by deconvolution of two Gaussian shaped peaks centered at 38.2 and 44.4° and corrected by instrumental broadening. A cluster size of 1.9 nm has been obtained that is smaller than the 2.4 nm value obtained by HR-TEM measurements. Differences of this kind have been reported for other gold nanoparticles when the sizes are measured by TEM[34] and mass spectrometry[35] techniques.

The results of thermogravimetric analysis of free 6MP molecules and 6MP-MPCs are shown in Figure 4. For 6MP molecules, two endothermic peaks appeared at 134 and 169 °C coinciding with the first weight loss of the thermogravimetric curve. This loss amounts to 11% of the total weight and should correspond to the water molecule that is bound to 6MP. The next peak at 324 °C takes place with a loss of around 19% of weight, and finally, the rest of the molecule disappears, and at the same time, a broad exothermic peak at 640 °C that should correspond to the combustion of the rest of the molecule is observed. Compared to the free 6MP molecules, the 6MP-MPCs

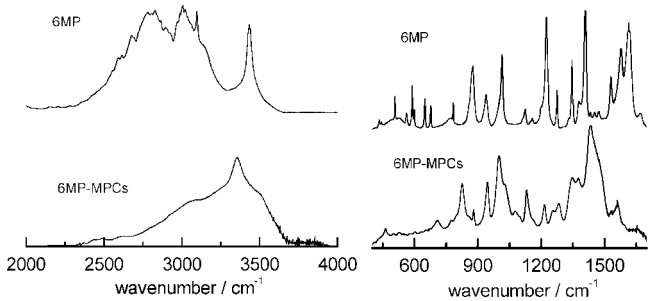

Figure 5. FT-IR absorption spectra of free 6MP and 6MP-MPCs at high and low wavenumber ranges.

exhibit somewhat different thermal properties. However, the transition regions revealed the same mass loss processes. TGA data showed that the weight loss for the 6MP-MPCs was only 9%. Assuming that this loss corresponds only to the 6MP molecules that form the monolayer and combining the data with the TEM diameter, the number of ligands on each nanocluster can be calculated along with the surface coverage and 6MP molecule footprint. In order to make these calculations, the gold nucleus can be modeled either as a sphere[33,36] or as a polyhedron.[33] The spherical model assumes that the gold core is a sphere with the same density as the bulk Au (19.3 g/cm^3) that is covered by a "skin" of hexagonally close-packed gold atoms.[36] On the other hand, the polyhedron model assumes that the sizes of the Au clusters reflect a discrete sequence of fcc structures of truncated octahedral shape,[32] characterized by a diameter which is associated with one of the "magic numbers" of Au atoms.[32,33] The analysis of the TGA data gives similar values for surface coverage (0.31 and 0.27) and number of ligands (62 or 63) by using the spherical or the polyhedron models. These values are higher than the surface coverage of 0.24 obtained for a 2D-6MP-SAM on Au(111) single crystal surface,[20] in agreement to what has been found for alkanethiolate MPCs. In the case of alkanethiolate ligands, the values obtained are almost double than those corresponding to SAMs formed on extended gold surfaces.[33,36−38] This fact has been explained as being due to the curvature of the nanoclusters that allows a better packing of the molecule chains with respect to flat gold surfaces. The consequence of this is the decrease of the ligand molecule footprint on going from 2D-SAM to MPCs. Thus, the 6MP footprint obtained is 23 Å^2 that is smaller than the 29 Å^2 (this value is close to the calculated using a molecular model) obtained by electrochemical techniques in 2D-SAMs,[20] although the difference is not as large as that found for alkanethiols and peptides. The different behavior should originate on the higher size of the 6MP-MPCs studied in this work in comparison to those where an extremely well-packed layer is possible due to the smaller cluster and molecule sizes.[33,36,38]

The IR spectra of the free 6MP and 6MP-MPCs are plotted in Figure 5. There are important differences between these spectra that can be analyzed by taking into account the band assignation made by Lapinski et al.[39]

The N−H stretching vibrations corresponding to the different 6MP tautomers are predicted in the high wavenumber region from 3480 to 3600 cm^{-1}, and as can be observed, they appear as a broad band centered at 3435 cm^{-1}. This band changes to 3350 cm^{-1} upon adsorption of the 6MP to the gold nanocluster surface. Following this region, a structured broad band that should contain the C−H stretching bands of the 6MP together with those of residual water are obtained. In this envelop a band at around 2670 cm^{-1} can be observed that corresponds to the S−H stretching of the thiol tautomers. In comparison, the spectrum of the 6MP-MPCs shows a structureless shoulder that points to the disappearance of those vibrations including that of the S−H group. The absence of this latter band can be considered as an indication of the interaction of the 6MP with the gold surface through the sulfur atom.

The low frequency region of the spectra is even more complex. However, there are some details that deserve to be considered. Thus, in the spectrum corresponding to the free 6MP, bands at 505, 533, 560, and 584 cm^{-1} assigned to the N−H bending vibrations and at 649 and 677 cm^{-1} assigned to ring vibrations of the thiol and thione tautomers are observed. All of these bands disappear in the spectrum of the 6MP-MPCs. The metal-surface selection rule predicts that some infrared absorption bands should be absent from the spectra of molecules adsorbed on metal particles.[40] Thus, those bands corresponding to molecular vibrations with an oscillating dipole moment parallel to the surface should be suppressed for particles of sizes higher than 2 nm. Thus, the features observed in this system points to the fact that the molecules that form the protective layer should maintain a common orientation.

On the other hand, the band at 784 cm^{-1} that corresponds to a ring vibration is maintained in the adsorbed state, and moreover, an important band at 824 cm^{-1} not reported for any species in free 6MP appears in the spectrum of 6MP-MPCs. This band may correspond to a ring vibration that should be favored in the actual organized state of the adsorbed molecules.

An interesting feature observed is the change of the bands at 1002 and 1018 cm^{-1} that involve C−N stretching of the thiol and thione species, respectively, together with C−S stretching. The intensity of the 1002 cm^{-1} band increases in a parallel way with the decrease of the 1018 cm^{-1} band indicating the transformation of the different 6MP tautomers into the thiol species in the adsorbed state. This reasoning is also valid for the behavior of the bands in the region of 1340−1470 cm^{-1}, that is, a decrease in some bands concomitantly with the increase in the intensity of others, in particular, the one at 1458 cm^{-1}, indicating the presence of the thiol tautomer with a protonated N(9) in the adsorbed state.

Finally, the rest of bands at 1526, 1578, and 1615 cm^{-1} that coincide with these of the thione N(9)H (1512 and 1539 cm^{-1}), the thiol N(9)H (1544 and 1580 cm^{-1}), and the thiol N(7)H (1554 and 1619 cm^{-1}) are transformed into an unique band at 1562 cm^{-1}, in agreement with the presence of the thiol N(9)H species in the adsorbed state.

To gain a better understanding on the immobilization of the 6MP molecules on the nanocluster surface, the 6MP-MPCs were examined using XPS. In this experiment a pellet of clean 6MP-MPCs was formed and the XPS signal obtained for Au 4f, S 2p, and N 1s are plotted in Figure 6.

The Au 4f level is characterized by a sharp doublet having a peak to peak separation of 3.6 eV and a full width at half-maximum of 1.6 eV. The Au ($4f_{7/2}$) peak shows a binding energy (BE) of 84.0 eV, which is the typical value expected when thiolate monolayers self-assemble onto gold nanoclusters or extended gold surfaces.[33,41−43] These results are consistent with the Au^0 oxidation state. However, in a more detailed examination, it can be deduced that the peak can be resolved into two peaks (inset, Figure 6, top) located at 84 and 85.2 eV that amounts 85 and 15% of the total peak area, respectively. The low BE component may be assigned to the electron emission from Au^0, whereas the high BE component should correspond to the gold atoms in the Au^I oxidation state.[44−47] As described above, the gold nanoparticle is surrounded by 62 6MP molecules that may interact with some of the gold atoms

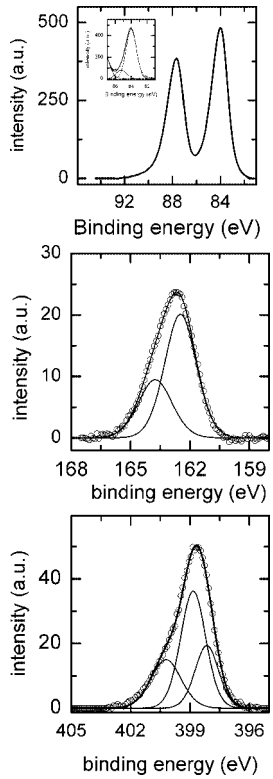

Figure 6. XPS spectra of 6MP-MPCs. Au 4f (top), S 2p (middle), and N 1s (bottom).

in the surface forming a layer of gold "staple" motifs. This layer should act as the protective layer for the core constituted by the rest of the gold atoms.[25,28,48] This would imply that the gold atoms in the cluster are in two distinct chemical states: the core Au atoms are in a metallic (charged neutral) state, whereas those forming the R−S(Au−SR)$_x$ oligomeric units (staple motifs) are oxidized.[48]

The S region consists of a rather broad and slightly asymmetric peak centered around 162.7 eV. It can be deconvoluted with a doublet, with an intensity ratio of 2:1 and a splitting of 1.2 eV, and the BEs of the S $2p_{3/2}$ and S $2p_{1/2}$ were 162.5 and 163.7 eV, respectively, in agreement with the values obtained for thiols strongly interacting with gold in 2D and 3D SAMs.[33,41,43,49−51]

Finally, the N (1s) spectrum shows a broad peak centered at 398.7 eV. The N (1s) BEs for nitrogen-containing heteroatomic compounds vary largely. In pyridine, for instance, the BE found is 398.0 eV[52] for the N(1s) in the neutral state, whereas the value for the protonated N is 400.2 eV. In the present case, the deconvolution of the N (1s) signal can be made with three Gaussian curves (Figure 5). If we consider the presence of different N atoms in the 6MP molecules, we can interpret this result as being due to the existence of three different N's with BEs of 398.1, 398.8, and 400.2 eV with an area ratio of 1:2:1, respectively. Thus, the peaks should correspond to the N(7) (at 398.1 eV), N(1) and N(3) (at 398.8 eV), and N(9)H (at 400.2 eV). In fact, N(7) should be similar to N(1) and N(3) as demonstrated by their BE values, and the N(9) possesses a higher BE (around 1.4 or 2 eV) due to the protonation. This reasoning is in agreement with reported results for mercaptopyridine adsorbed on gold surfaces.[53]

These results, therefore, indicate the presence of the thiol N(9)H tautomer as the only species in the monolayer protecting the gold nanocluster in agreement with the results of FTIR spectroscopy described above.

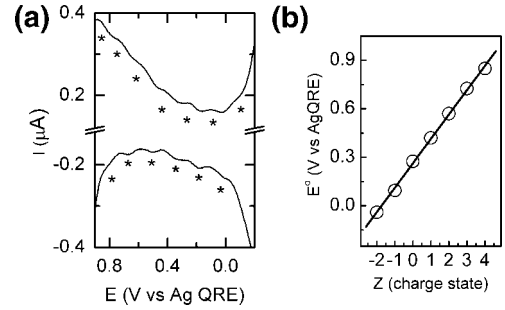

Figure 7. DPV curves of 6MP-MPCs in 0.1 M Bu_4NPF_6/DMF solution (a). The charge state variations with peak potentials (*Z* plot) (b).

Electrochemical Behavior of 6MP-MPCs. The characterization of the 6MP-MPCs described in this work shows that these gold nanoclusters are somewhat monodisperse and possess certain stability in solvents as DMF. This is mainly due to the chemical properties of the protecting layer. In this sense, as reported for the 6MP-AuNPs of 13 nm diameter,[23] the preferred solvents are aqueous solutions or some high and medium dielectric constant organic solvents. We have tried to dissolve the 6MP-MPCs in different solvents, and we have found that DMF is the most appropriate since it maintains the suspension stable to carry out experimental measurements.

This fact has encouraged us to probe the voltammetry of the 6MP-MPCs in DMF as a solvent in order to check the quantized double layer (QDL) charging of these nanoclusters. Figure 7 shows the typical differential pulse voltammetry response of the 6MP-MPCs on a Pt electrode where 6 (negative going scan) or 7 (positive going scan) evenly spaced ($\Delta V \approx 0.16$ V) peak characteristics of charge injection to the metal core are obtained. The consecutive one electron QDL peaks observed can be taken as the formal redox potential $E°'$ and can be described by

$$E_{Z,Z-1} = E_{PZC} + \frac{(Z - 1/2)e}{C_{CLU}} \qquad (2)$$

where E_{PZC} is the potential of zero charge of the MPC, Z is assigned such that $Z > 0$ and $Z < 0$ correspond to core oxidation and reduction, respectively, and C_{CLU} is the capacitance of the MPC. This equation predicts a linear plot of the formal redox potential vs charge state (Z plot) which can be used to determine C_{CLU} from the slope.[54−60] In Figure 7b, we have plotted the $E°'$ measured in the DPV (Figure 6a), and as can be seen, they follow a linear variation with a slope that allows us determine a C_{CLU} value of 1.06 aF. Typically, the spacing between the peaks at 0.27 and 0.09 V is greater than those of the rest of the peaks that remain constants. We have assumed that this feature is related with the capacitance minimum that takes place at the potential of zero charge (pzc).[56,61]

The capacitance value is in good agreement with the theoretically estimated capacitance value of 1.1 aF using a concentric sphere capacitance model, as

$$C_{CLU} = 4\pi\varepsilon_0\varepsilon_r\left(\frac{r}{d}\right)(r + d) \qquad (3)$$

where ε_0 is the permittivity of the free space, ε_r is the relative permittivity of the protecting monolayer (taken as 3.4), r is the radius of the MPC core (1.2 nm), and d is the length of the protecting molecule (0.8−0.9 nm[20]). The relative permittivity of the 6MP-protecting monolayer has been determined by

measuring the double layer capacitance of a 6MP-SAM on Au(111) single crystal electrode in contact with a DMF solution and considering the parallel-plate capacitor model.

At this point, it is interesting to note that the 6MP protecting monolayer confers a highly polar character to the MPCs in a way that makes them stable in aqueous solutions. However, they are also soluble in some organic solvents as is evidenced in this work.

The absence of QDL charging voltammetry in MPCs with highly polar ligands[12,16,62] has been explained as a result of the great decrease in ΔV as the effective dielectric constant of the ligands increases.[4] In this sense, the 6MP-MPCs have a dual behavior since, on one hand, they possess the appropriate polarity to be soluble in aqueous solutions but, on the other hand, the effective dielectric constant of the 6MP monolayer is low enough to allow the QDL charging of the MPC. In fact, if the important dipole moment of the 6MP molecule[39] is taken into account, then the monolayer should be considered as an array of dipoles that should interact with the dipole moment of the DMF molecules near the surface, a phenomenon that would contribute to lower the double layer capacitance of the protecting layer ($\sim 4-5\ \mu F/cm^2$) [63,64] with respect to that found for the same SAM in contact with other solvents.

On the other hand, it has been reported[65,66] that the redox behavior of MPCs suffers dramatic changes when some of the nonpolar ligands are exchanged for ligands that possess oriented dipole moments. This fact implies a pronounced effect on the electron-donating or accepting properties on the underlying metal substrate that results in a systematic shift of the voltammetric formal potentials toward more positive values with increasingly electron withdrawing properties. The observed shift in the different peaks is approximately equal, so that the peak separation remains unchanged. This potential displacement of the DPV peaks must be responsible for the value of the pzc ($\sim$0.175 V) of the 6MP-MPCs obtained in this work.

Conclusions

The synthesis of 6MP-MPCs in DMF yields nanoclusters of a moderately monodisperse size of 2.4 ± 0.5 nm with an average stoichiometry of $Au_{459}(6MP)_{62}$ as determined by thermogravimetric analysis. These MPCs are soluble in DMF and alkaline aqueous solutions and, as it occurs with alkenethiols-MPCs, they can be repeatedly isolated and redissolved without aggregation.

The sharp distribution of sizes of these 6MP-MPCs is due not only to the high affinity of the thiol group with the gold surface but also to the strong lateral interactions of the purine ring that take place upon adsorption of the molecules on the nascent clusters surfaces, thus avoiding further growth of the nanoparticles.

The fast equilibrium thione-thiol facilitates the transformation of the solution species into the thiol species in the adsorbed state. In this sense, the FTIR together with the XPS results point to the interaction of the 6MP molecule with the gold surface through the S atom and to the thiol N(9)H as the only species in the 6MP monolayer protecting the gold clusters.

The 6MP-MPCs synthesized in this work show QDL charging voltammetry in DMF, and the capacitance value determined is 1.06 aF. As far as we know, this is the first time that a QDL response is reported for nanoclusters protected with polar ligands. In this sense, the low effective relative permittivity of the 6MP monolayer in contact with a DMF solution should be responsible for the small MPC capacitance of these nanoclusters, and thus, the voltage intervals between sequential single electron changes in their core charges are detectable by voltammetric means at room temperature.

Acknowledgment. We thank the Ministerio de Educación y Ciencia (MEC) (Projects CTQ2004-00977 and CTQ2007-62723/BQU) Junta de Andalucía and University of Córdoba for financial support of this work. A.J.V. acknowledges the MEC for a fellowship of the FPU program.

References and Notes

(1) Schmid, G. *Chem. Rev.* **1992**, *92*, 1709.
(2) Daniel, M. C.; Astruc, D. *Chem. Rev.* **2004**, *104*, 293.
(3) Shipway, A. N.; Katz, E.; Willner, I. *ChemPhysChem* **2000**, *1*, 18.
(4) Murray, R. W. *Chem. Rev.* **2008**, *108*, 2688.
(5) Brust, M.; Walker, M.; Bethell, D.; Schiffrin, D. J.; Whyman, R. *J. Chem. Soc.- Chem. Commun.* **1994**, 801.
(6) Hostetler, M. J.; Green, S. J.; Stokes, J. J.; Murray, R. W. *J. Am. Chem. Soc.* **1996**, *118*, 4212.
(7) Ingram, R. S.; Hostetler, M. J.; Murray, R. W. *J. Am. Chem. Soc.* **1997**, *119*, 9175.
(8) Templeton, A. C.; Hostetler, M. J.; Kraft, C. T.; Murray, R. W. *J. Am. Chem. Soc.* **1998**, *120*, 1906.
(9) Templeton, A. C.; Hostetler, M. J.; Warmoth, E. K.; Chen, S. W.; Hartshorn, C. M.; Krishnamurthy, V. M.; Forbes, M. D. E.; Murray, R. W. *J. Am. Chem. Soc.* **1998**, *120*, 4845.
(10) Schaaff, T. G.; Knight, G.; Shafigullin, M. N.; Borkman, R. F.; Whetten, R. L. *J. Phys. Chem. B* **1998**, *102*, 10643.
(11) Schaaff, T. G.; Whetten, R. L. *J. Phys. Chem. B* **2000**, *104*, 2630.
(12) Templeton, A. C.; Cliffel, D. E.; Murray, R. W. *J. Am. Chem. Soc.* **1999**, *121*, 7081.
(13) Negishi, Y.; Nobusada, K.; Tsukuda, T. *J. Am. Chem. Soc.* **2005**, *127*, 5261.
(14) Choi, M. M. F.; Douglas, A. D.; Murray, R. W. *Anal. Chem.* **2006**, *78*, 2779.
(15) Wolfe, R. L.; Murray, R. W. *Anal. Chem.* **2006**, *78*, 1167.
(16) Templeton, A. C.; Chen, S. W.; Gross, S. M.; Murray, R. W. *Langmuir* **1999**, *15*, 66.
(17) Huang, T.; Murray, R. W. *J. Phys. Chem. B* **2001**, *105*, 12498.
(18) Brust, M.; Fink, J.; Bethell, D.; Schiffrin, D. J.; Kiely, C. *J. Chem. Soc. Chem. Commun.* **1995**, 1655.
(19) Madueno, R.; Sevilla, J. M.; Pineda, T.; Roman, A. J.; Blazquez, M. *J. Electroanal. Chem.* **2001**, *506*, 92.
(20) Madueno, R.; Pineda, T.; Sevilla, J. M.; Blazquez, M. *Langmuir* **2002**, *18*, 3903.
(21) Madueno, R.; Pineda, T.; Sevilla, J. M.; Blazquez, M. *J. Phys. Chem. B* **2005**, *109*, 1491.
(22) Madueno, R.; Garcia-Raya, D.; Viudez, A. J.; Sevilla, J. M.; Pineda, T.; Blazquez, M. *Langmuir* **2007**, *23*, 11027.
(23) Viudez, A. J.; Madueno, R.; Pineda, T.; Blazquez, M. *J. Phys. Chem. B* **2006**, *110*, 17840.
(24) Turkevic, J.; Kim, G. *Science* **1970**, *169*, 873.
(25) Jadzinsky, P. D.; Calero, G.; Ackerson, C. J.; Bushnell, D. A.; Kornberg, R. D. *Science* **2007**, *318*, 430.
(26) Whetten, R. L.; Price, R. C. *Science* **2007**, *318*, 407.
(27) Hakkinen, H.; Walter, M.; Gronbeck, H. *J. Phys. Chem. B* **2006**, *110*, 9927.
(28) Heaven, M. W.; Dass, A.; White, P. S.; Holt, K. M.; Murray, R. W. *J. Am. Chem. Soc.* **2008**, *130*, 3754.
(29) Brauer, G. *Handbook of Preparative Inorganic Chemistry*; Academic Press: New York, 1965.
(30) Bayliss, P. *Mineral Powder Diffraction File Data Book*; JCPDS: Swarthmore, PA, 1986.
(31) Seo, D.; Park, J. C.; Song, H. *J. Am. Chem. Soc.* **2006**, *128*, 14863.
(32) Whetten, R. L.; Khoury, J. T.; Alvarez, M. M.; Murthy, S.; Vezmar, I.; Wang, Z. L.; Stephens, P. W.; Cleveland, C. L.; Luedtke, W. D.; Landman, U. *Adv. Mater.* **1996**, *8*, 428.
(33) Hostetler, M. J.; Wingate, J. E.; Zhong, C. J.; Harris, J. E.; Vachet, R. W.; Clark, M. R.; Londono, J. D.; Green, S. J.; Stokes, J. J.; Wignall, G. D.; Glish, G. L.; Porter, M. D.; Evans, N. D.; Murray, R. W. *Langmuir* **1998**, *14*, 17.
(34) Solliard, C. *Surf. Sci.* **1981**, *106*, 58.
(35) Vezmar, I.; Alvarez, M. M.; Khoury, J. T.; Salisbury, B. E.; Shafigullin, M. N.; Whetten, R. L. *Z. Phys. D* **1997**, *40*, 147.
(36) Terrill, R. H.; Postlethwaite, T. A.; Chen, C. H.; Poon, C. D.; Terzis, A.; Chen, A. D.; Hutchison, J. E.; Clark, M. R.; Wignall, G.; Londono, J. D.; Superfine, R.; Falvo, M.; Johnson, C. S.; Samulski, E. T.; Murray, R. W. *J. Am. Chem. Soc.* **1995**, *117*, 12537.
(37) Widrig, C. A.; Alves, C. A.; Porter, M. D. *J. Am. Chem. Soc.* **1991**, *113*, 2805.

(38) Fabris, L.; Antonello, S.; Armelao, L.; Donkers, R. L.; Polo, F.; Toniolo, C.; Maran, F. *J. Am. Chem. Soc.* **2006**, *128*, 326.

(39) Lapinski, L.; Nowak, M. J.; Kwiatkowski, J. S.; Leszczynski, J. *J. Phys. Chem. A* **1999**, *103*, 280.

(40) Greenler, R. G.; Snider, D. R.; Witt, D.; Sorbello, R. S. *Surf. Sci.* **1982**, *118*, 415.

(41) Bourg, M. C.; Badia, A.; Lennox, R. B. *J. Phys. Chem. B* **2000**, *104*, 6562.

(42) Heister, K.; Zharnikov, M.; Grunze, M.; Johansson, L. S. O. *J. Phys. Chem. B* **2001**, *105*, 4058.

(43) Joseph, Y.; Besnard, I.; Rosenberger, M.; Guse, B.; Nothofer, H. G.; Wessels, J. M.; Wild, U.; Knop-Gericke, A.; Su, D.; Schlogl, R.; Yasuda, A.; Vossmeyer, T. *J. Phys. Chem. B* **2003**, *107*, 7406.

(44) King, D. E. *J. Vac. Sci. Technol. A* **1995**, *13*, 1247.

(45) Vandevondel, D. F.; Vanderkelen, G. P.; Schmidbaur, H.; Wolleben, A.; Wagner, F. E. *Phys. Scr.* **1977**, *16*, 364.

(46) Bhargava, S. K.; Mohr, F.; Gorman, J. D. *J. Organomet. Chem.* **2000**, *607*, 93.

(47) Raptis, R. G.; Porter, L. C.; Emrich, R. J.; Murray, H. H.; Fackler, J. P. *Inorg. Chem.* **1990**, *29*, 4408.

(48) Walter, M.; Akola, J.; Lopez-Acevedo, O.; Jadzinsky, P. D.; Calero, G.; Ackerson, C. J.; Whetten, R. L.; Gronbeck, H.; Hakkinen, H. *Proc. Natl. Acad. Sci. U.S.A.* **2008**, *105*, 9157.

(49) Clegg, R. S.; Reed, S. M.; Smith, R. K.; Barron, B. L.; Rear, J. A.; Hutchison, J. E. *Langmuir* **1999**, *15*, 8876.

(50) Uvdal, K.; Petoral, R. M. *J. Phys. Chem. B* **2003**, *107*, 13396.

(51) Cavalleri, O.; Oliveri, L.; Daccà, A.; Parodi, R.; Rolandi, R. *Appl. Surf. Sci.* **2001**, *175*−*176*, 357.

(52) Hendrickson, D. N.; Hollander, J. M.; Jolly, W. L. *Inorg. Chem.* **1969**, *8*, 2642.

(53) Zhou, W. P.; Baunach, T.; Ivanova, V.; Kolb, D. M. *Langmuir* **2004**, *20*, 4590.

(54) Ingram, R. S.; Hostetler, M. J.; Murray, R. W.; Schaaff, T. G.; Khoury, J. T.; Whetten, R. L.; Bigioni, T. P.; Guthrie, D. K.; First, P. N. *J. Am. Chem. Soc.* **1997**, *119*, 9279.

(55) Chen, S. W.; Ingram, R. S.; Hostetler, M. J.; Pietron, J. J.; Murray, R. W.; Schaaff, T. G.; Khoury, J. T.; Alvarez, M. M.; Whetten, R. L. *Science* **1998**, *280*, 2098.

(56) Quinn, B. M.; Liljeroth, P.; Ruiz, V.; Laaksonen, T.; Kontturi, K. *J. Am. Chem. Soc.* **2003**, *125*, 6644.

(57) Pietron, J. J.; Hicks, J. F.; Murray, R. W. *J. Am. Chem. Soc.* **1999**, *121*, 5565.

(58) Chen, S. W.; Murray, R. W.; Feldberg, S. W. *J. Phys. Chem. B* **1998**, *102*, 9898.

(59) Miles, D. T.; Murray, R. W. *Anal. Chem.* **2003**, *75*, 1251.

(60) Li, D.; Li, J. H. *Chem. Phys. Lett.* **2003**, *372*, 668.

(61) Chen, S. W.; Murray, R. W. *J. Phys. Chem. B* **1999**, *103*, 9996.

(62) Gittins, D. I.; Bethell, D.; Schiffrin, D. J.; Nichols, R. J. *Nature* **2000**, *408*, 67.

(63) Graupe, M.; Takenaga, M.; Koini, T.; Colorado, R.; Lee, T. R. *J. Am. Chem. Soc.* **1999**, *121*, 3222.

(64) Subramanian, S.; Sampath, S. *J. Colloid Interface Sci.* **2007**, *313*, 64.

(65) Holm, A. H.; Ceccato, M.; Donkers, R. L.; Fabris, L.; Pace, G.; Maran, F. *Langmuir* **2006**, *22*, 10584.

(66) Guo, R.; Murray, R. W. *J. Am. Chem. Soc.* **2005**, *127*, 12140.

JP810720T